



Article

Insight into the Ex Situ Catalytic Pyrolysis of Biomass over Char Supported Metals Catalyst: Syngas Production and Tar Decomposition

Mian Hu ^{1,2}, Baihui Cui ³, Bo Xiao ², Shiyi Luo ⁴ and Dabin Guo ^{2,*}¹ College of Environment, Zhejiang University of Technology, Hangzhou 310032, China; mianhu@zjut.edu.cn² School of Environmental Science & Engineering, Huazhong University of Science and Technology, Wuhan 430074, China; xiaobo1958@126.com³ Institute of Hydrobiology, Chinese Academy of Sciences, Wuhan 430072, China; cuibaihui@ihb.ac.cn⁴ State Key Laboratory of Physical Chemistry of Solid Surfaces, College of Chemistry and Chemical Engineering, Xiamen University, Xiamen 361005, China; luoshiyi@xmu.edu.cn

* Correspondence: dabin@hust.edu.cn

Received: 8 June 2020; Accepted: 14 July 2020; Published: 18 July 2020



Abstract: Ex situ catalytic pyrolysis of biomass using char-supported nanoparticles metals (Fe and Ni) catalyst for syngas production and tar decomposition was investigated. The characterizations of fresh Fe-Ni/char catalysts were determined by TGA, SEM-EDS, Brunauer-Emmett-Teller (BET), and XPS. The results indicated that nanoparticles metal substances (Fe and Ni) successfully impregnated into the char support and increased the thermal stability of Fe-Ni/char. Fe-Ni/char catalyst exhibited relatively superior catalytic performance, where the syngas yield and the molar ratio of H₂/CO were 0.91 Nm³/kg biomass and 1.64, respectively. Moreover, the lowest tar yield (43.21 g/kg biomass) and the highest tar catalytic conversion efficiency (84.97 wt.%) were also obtained under the condition of Ni/char. Ultimate analysis and GC-MS were employed to analyze the characterization of tar, and the results indicated that the percentage of aromatic hydrocarbons appreciably increased with the significantly decrease in oxygenated compounds and nitrogenous compounds, especially in Fe-Ni/char catalyst, when compared with no catalyst pyrolysis. After catalytic pyrolysis, XPS was employed to investigate the surface valence states of the characteristic elements in the catalysts. The results indicated that the metallic oxides (Me_xO_y) were reduced to metallic Me⁰ as active sites for tar catalytic pyrolysis. The main reactions pathway involved during ex situ catalytic pyrolysis of biomass based on char-supported catalyst was proposed. These findings indicate that char has the potential to be used as an efficient and low-cost catalyst toward biomass pyrolysis for syngas production and tar decomposition.

Keywords: ex situ; catalytic pyrolysis; biomass; syngas production; tar decomposition

1. Introduction

In recent years, biomass has attracted much attention mainly because it can be used as a renewable resource to produce various high-quality chemicals, multi-functional char-based materials, and fuel products, which can not only reduce the burden of relying on fossil resources, but also are regarded as a meaningful way toward CO₂ emissions [1–6]. Currently, biomass energy accounts for about 9% of the world's total energy supply that plays a key role in tackling issues of energy-supply security and environmental problems [7]. Some promising thermochemical conversion processes, such as pyrolysis, gasification, hydrothermal liquefaction etc., have been explored toward enhanced energy and resource recovery from biomass [8–11]. Among them, pyrolysis is recognized as an advanced and

practical technology for high-value utilization of the biomass [12,13]. Generally, pyrolysis of organic substances produces three phases of matter. It produces gaseous products, including syngas, methane, short hydrocarbon chain gases, and carbon dioxide. It also produces liquid and carbon products [14]. However, during the pyrolysis process, some unpleasant by-products (e.g., tar, NO_x , and ash) are inevitably produced. Tar, which generally includes aromatic compounds with one-ring to five-rings, oxygen-containing hydrocarbons, and polycyclic aromatic hydrocarbons, is one of the main problems hindering the industrialization of pyrolysis technology, because it condenses easily [15–17].

Catalytic pyrolysis is an effective route to improve tar quality, which makes pyrolysis volatiles occur in a series of secondary reactions, and make the heavier component split into light oil and gas, as well as transform the oxygen in tar to CO_2 , CO, and H_2O through decarboxylation, decarbonylation, and dehydration reactions, respectively [18,19]. In addition, the introduction of a catalyst in the pyrolysis process can reduce the activation energy of the reaction, thereby greatly reducing the required pyrolysis temperature [20,21]. Generally, the catalytic pyrolysis can be classified into in situ and ex situ configurations according to the location of the catalyst. In situ catalytic pyrolysis means that the catalyst and feedstock are mixed together, and the pyrolysis and vapor catalytic reforming/cracking processes take place in the same reactor; therefore, the capital and operating costs are reduced. Ex situ catalytic pyrolysis means that the catalyst and feedstock are loaded separately in different reactors. The pyrolysis vapor flows out from the pyrolysis reactor and introduces into the catalytic reactor for catalytic reforming/cracking [22,23]. Compared with the in situ catalytic pyrolysis, the ex situ catalytic pyrolysis can adjust the temperature of the pyrolysis reactor and catalytic reactor, respectively, making the reaction system more controllable and flexible. Meanwhile, the probability of contact between pyrolysis vapors and catalyst is higher in an ex situ catalytic pyrolysis system. In addition, compared with in situ catalytic pyrolysis, the post-reaction catalyst can be easily separated for next cycle [24]. Various char-based catalysts were developed by Han et al., [25] for the ex situ catalytic upgrading of coal pyrolysis tar and the results exhibited that the catalytic upgrading resulted in a lower total yield of tar and a higher yield of non-condensable gas. Gamliel et al. [26] performed a comparison between in situ and ex situ catalytic fast pyrolysis, and the results indicated that the ex situ catalytic fast pyrolysis produced more gases yield and aromatics in the bio-oil than in situ catalytic fast pyrolysis. Depending on the above statement, thus, in this study, the ex situ catalytic pyrolysis system was self-designed for investigation of biomass pyrolysis.

Various catalysts, such as nickel-based catalysts [27], noble-metal-based catalysts [28], transition metal catalysts [29], alkali metal catalysts [30], natural catalysts [31], zeolite catalysts [32], and carbon-supported catalysts [33] have been investigated for syngas production and tar decomposition from biomass. In general, Ni-based catalysts are considered to be better for catalytic cracking/reforming of tar. Ni metal catalysts can not only activate hydrogen, but also significantly inhibit the polymerization of unsaturated hydrocarbons that lead to coke formation. However, compared with Ni-based catalysts, Fe-based catalysts are much cheaper, more abundant, and more environmentally friendly. Moreover, iron oxides have a variety of different physicochemical properties, such as Fe_2O_3 and Fe_3O_4 , which may increase catalytic activity or reduce coking deposition. Moreover, the mono- or bi-metallic catalysts, such as Fe-Ni/HZSM-5 [34], Co-Fe/ Al_2O_3 [35], and Ni/char [8] are beneficial for tar decomposition. Catalyst supports are usually supported by metal oxides or natural minerals, and these supports are relatively expensive. The nature of a catalyst support plays an important role in the reactivity of the catalyst. Char, as a low-cost porous pyrolysis residue, is considered to be an effective catalyst/support in tar removal, due to its inherent catalytic alkali and alkaline earth metallic species, as well as the defected carbon structural units in chars [36,37]. Meanwhile, the porous structure of char facilitates metal impregnation and makes tar more accessible to catalytic active sites. Hence, char, which could easily be obtained from solid waste pyrolysis, may have the potential to upgrade the bio-oil quality and syngas yield. However, although this cheap and green char catalyst has received more attention on catalytic pyrolysis of biomass, it is still worth it to understand the catalytic activities and mechanisms of char or char-supported catalysts on tar decomposition and syngas production.

In this work, ex situ catalytic pyrolysis of biomass over char-supported Ni and/or Fe catalysts for syngas production and tar decomposition was investigated. The objectives of this study were to (1) synthesize char-based catalysts by impregnation with metal (Fe and/or Ni), (2) compare the catalytic activity of char-based catalysts for syngas production and tar decomposition, and (3) discuss the catalytic mechanism of biomass over char-based catalyst.

2. Materials and Methods

2.1. Pyrolysis Feedstock

Pine sawdust (PS) used in this study was collected from a factory in Wuhan, China. Sun-drying for 7 days was performed for PS, to reduce the moisture content; then it was crushed and sieved to obtain a particle size <0.107 mm before using. Detailed information about the sample is listed in Table 1. $\text{Fe}(\text{NO}_3)_3 \cdot 9\text{H}_2\text{O}$ and $\text{Ni}(\text{NO}_3)_2 \cdot 6\text{H}_2\text{O}$ chemicals employed for the catalyst synthesized were analytical reagent grade.

Table 1. Ultimate and proximate analyses of pine sawdust (PS) and char samples ^b.

	Proximate Analysis (wt.%)				Ultimate Analysis (wt.%)				S_{BET} (m^2/g)	
	M	A	V	FC	C	H	O ^a	N		S
PS	9.18	1.25	74.46	15.11	46.36	5.75	45.3	2.26	0.35	5.24
Char	3.04	10.4	5.45	81.11	76.12	1.01	8.12	2.54	0.27	252.13

Notes: M, moisture content; V, volatile matter; F, fixed carbon; A, ash; LHV, low heating value; S_{BET} , Brunauer–Emmett–Teller specific surface area. ^a By difference. ^b Air dry basis.

2.2. Catalysts Preparation

Char, as a catalyst or catalyst support, was derived from a biomass steam gasification system, and its main physicochemical properties are also shown in Table 1. Carbon content of char is 76.12 wt.% with limited oxygen (8.12 wt.%). The Brunauer–Emmett–Teller (BET) specific surface area is 252.13 (m^2/g), which should make it good as a catalyst support. Before being used as a catalyst support, char needs to be sieved (0.5–1 mm), washed, and dried (80 °C). Char-supported iron and nickel catalysts were prepared by impregnation method. Firstly, 44.0 g of char support was impregnated by using a mixed aqueous solution of $\text{Fe}(\text{NO}_3)_3 \cdot 9\text{H}_2\text{O}$ (21.6 g) and $\text{Ni}(\text{NO}_3)_2 \cdot 6\text{H}_2\text{O}$ (14.8 g), and stirred at room temperature for 12 h. After that, the sample was dried at 105 °C for 24 h. The prepared nanoparticles catalyst was marked as Fe-Ni/char catalyst. Meanwhile, char without metals was used as the baseline for comparison.

2.3. Apparatus and Procedure

In this study, the catalytic pyrolysis of different types of char and Ni-6/char was used as the catalyst. Ex situ catalytic pyrolysis of biomass was conducted in a self-built equipment, as shown in Figure 1. The reaction system consists of carrier gas unit, pyrolysis furnace, catalytic furnace, condenser, gas flow meter, and GC for gas analysis. Two quartz glass tubes (i.d. = 75 and 80 mm, effective length = 700 and 800 mm, respectively) were used as the pyrolysis and catalytic bed reactor, respectively.

The 5.0 g catalyst was preloaded into the catalytic bed, followed by protection by 0.1 L/min of N_2 for 20 min. The temperatures of the pyrolysis and catalytic reactors were both controlled at 800 °C. We loaded 5.0 g of PS onto a heat-resistant boat and pushed it into the middle of the pyrolysis reactor, when the desired temperature stabilized. The pyrolysis gas passed through a condenser, and a mixture liquid (tar and water) was obtained.

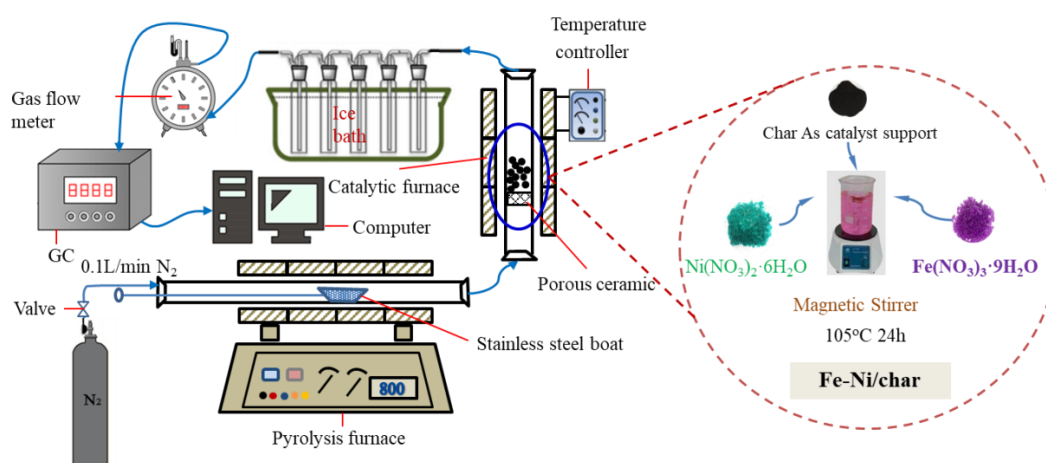


Figure 1. Schematic diagram of ex situ catalytic pyrolysis system.

Flow meter was employed to determine the volume of non-condensable syngas, and its composition was measured by a Gas Chromatography (GC).

After each experiment, the liquid products which came from the ice bath and connection tubes were collected. According to the standard ASTM D244 and IP 291.1 methods, water and tar were further separated. The mass of tar was weighted and recorded as the tar yield.

2.4. Method of Sampling and Analysis

The syngas was analyzed by using GC 9800T with a thermal conductivity detector. The column used was TDX-01 for the analysis of H_2 , CO , CO_2 , and CH_4 . The temperatures 200, 85, and 90 °C were employed, respectively, for the injector, oven, and detector. The argon was applied for carrier gas, while the standard gas mixtures were used for quantitative calibration.

BET specific surface area (S_{BET}) was determined by the Brunauer–Emmett–Teller (BET) equation. The total pore volume (V_{total}) was investigated by single point adsorption total pore volume analysis. Average pore diameter (D) was obtained by $4V/S_{BET}$ based on BET method. The thermal stability of fresh catalysts was characterized by the TG/DTA Synchronous analyzer (Diamond TG/DTA, PerkinElmer Instruments, Norwalk, CT, USA). Scanning electron microscopy (SEM) coupled with energy-dispersive X-ray fluorescence spectroscopy (EDX) with a Quanta 200 (FEI Company, Eindhoven, Nederland) was employed to examine the structural characteristics and elements distribution of catalysts. Before and after catalytic reforming, X-ray photoelectron spectroscopy (XPS, Shimadzu- Kratos GROUP PLC), using Al $K\alpha$ as an X-ray source, was applied to analyze the species of the elements. C 1s set as 285.0 eV was used as an internal standard.

Tar samples were analyzed by using an Agilent GC/MS (7890A/5975C, Agilent, Santa Clara, CA, USA) with a capillary column (HP-5MS) (30 m × 0.25 mm × 0.25 mm) to quantify the relatively light components of the tar. The identification of the peaks in the chromatogram were determined by using NIST98 mass library.

3. Results and Discussion

3.1. Characterization of Fresh Catalysts

Thermogravimetric analysis (TGA) was used to determine the thermal stability of fresh char and char-supported catalysts at a heating rate of 15 °C/min and N_2 flow rate of 100 mL/min, and the results are presented in Figure 2a. It can be seen that, when the temperature was above about 350 °C, the weight of char/char-supported catalysts decreased rapidly. Thermal decomposition resulted in the greatest mass loss in the temperature range of about 350–663 °C for char, which differed with Fe-Ni/char. The mass remaining, compared to the initial mass, is 89.42% for char, and 89.81% for

Fe-Ni/char, which indicated that the order of thermal stability of char and char supported catalysts is Fe-Ni/char > char.

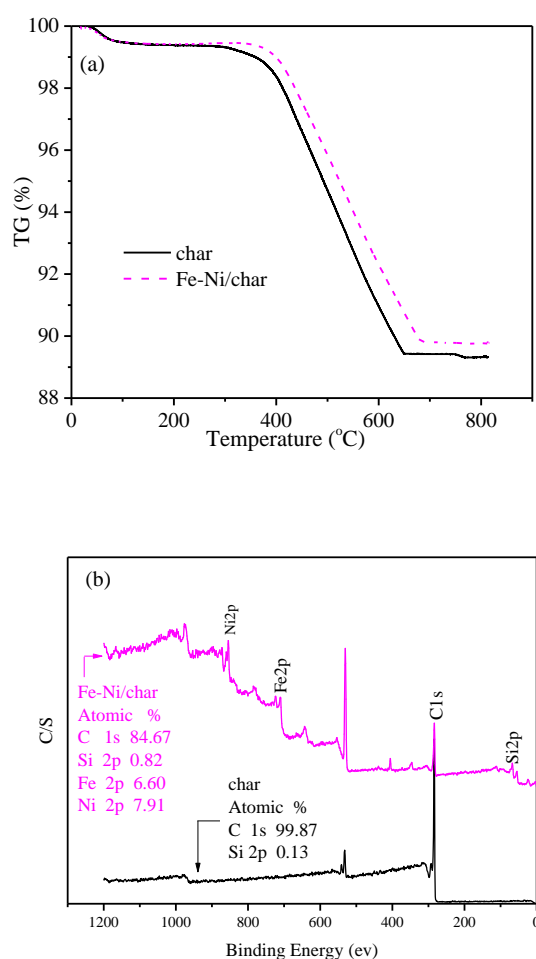


Figure 2. TG curves (a) and XPS (b) analysis of different fresh catalysts.

The SEM images of the fresh char and Fe-Ni/char catalysts with elements distribution by EDS analysis are shown in Supplementary Materials Figure S1. From the image in Supplementary Materials Figure S1a, it can be seen that the morphological characterizations of rough, corrugated, and many cavities are observed on the char samples, which can be proved by the result of specific surface areas ($252.13 \text{ m}^2/\text{g}$). Meanwhile, the EDS result of char indicated that some inorganic elements (such as silicon and potassium) existed on the surface of char. After Ni and Fe loading, small particles can be observed, and their specific surface areas accordingly decreased ($74.89 \text{ m}^2/\text{g}$ for Fe-Ni/char), as shown in Table 2. Additionally, the EDS results of the Fe-Ni/char catalyst are presented in Supplementary Materials Figure S1b and indicate that the metallic matters were successfully inserted into the char framework.

Table 2. Textural properties of fresh char and char-supported catalysts.

Sample.	BET Surface Area (S_{BET} : m^2/g)	Total Pore Volume (V_{total} : cm^3/g)	Average Pore Diameter (D: nm)
Char	252.13	0.20	3.56
Fe-Ni/char	74.89	0.06	2.42

The nitrogen adsorption–desorption isotherms and pore size distribution of different fresh catalysts were analyzed, and the results are shown in Supplementary Materials Figure S2. By analyzing the pore

diameter distribution of char, it can be seen that the influence of loading Fe and Ni on char structure reduces the average pore diameter of char. According to the Brunauer–Deming–Deming–Teller (BDDT) classification, the isotherms of char and Fe-Ni/char could be type IV, due to the porous walls covering the surface followed by pore filling associated with various hysteresis loops. The above results shown that char-based catalysts exhibited good catalytic activity during the catalytic pyrolysis process.

XPS analysis of catalysts was performed, and the results are shown in Figure 2b. The surface of the char was enriched with only carbon and oxygen (not given but really exist in the binding energy of about 529 eV) and a small amount of silicon, while Fe and Ni appear on the corresponding char-supported metal catalysts after impregnation. These results are consistent with the consequences of EDS analyses, which indicated that the Fe and Ni were successfully impregnated into the char support.

3.2. Syngas Yield and Composition

As a key precursor of fuel products, syngas has different applications, depending on the ratio of H_2/CO . When using dimethyl ether as the target product, the ratio is 1, while the synthesis of methanol and long-chain alkanes requires a ratio of 2 or higher [38]. However, the ratio of the H_2/CO in syngas is generally kept at a lower level, especially when air and oxygen are used as gasifying agents [39]. Biagini et al. [40] investigated the gasification of agricultural residues, and the results indicated that the H_2/CO ratio of the syngas was lower than 1. Weiland et al. [41] gasified the wood powder with oxygen, and the ratio of H_2/CO was between 0.54 and 0.57. Therefore, catalytic pyrolysis/gasification should be performed to increase the syngas H_2/CO ratio.

The syngas yield and composition from biomass catalytic pyrolysis processes under different employed catalysts are shown in Figure 3. Compared with the char as catalyst, the syngas yield is increased in the presence of the Fe-Ni/char catalyst. The increase in syngas production is mainly due to the complex thermochemical reactions between three phase products (gas, char, and tar) and the catalyst. More specifically, the syngas yield ($0.91 \text{ Nm}^3/\text{kg biomass}$) under the Fe-Ni/char catalyst is higher than in the case of the char catalyst, indicating that its catalytic performance for syngas production is better. Figure 3 also shown the content of the four main gas components, namely H_2 , CO, CO_2 , and CH_4 , under different catalysts. In comparison with the char as catalyst, the volume concentrations of H_2 and CO increased, whereas the CO_2 and CH_4 volume concentrations decreased in the presence of the Fe-Ni/char catalyst. The char-supported Fe and Ni catalyst exhibited much higher catalytic activity than char catalyst, which in turn promoted tar catalytic cracking and syngas generation. Meanwhile, under the different catalysts' conditions, the molar ratio of H_2/CO was 1.57 and 1.64, respectively, for char and Fe-Ni/char. Therefore, the syngas obtained from these char and Fe-Ni/char catalysts can act as feedstock for Fischer–Tropsch synthesis for the production transportation fuels [42].

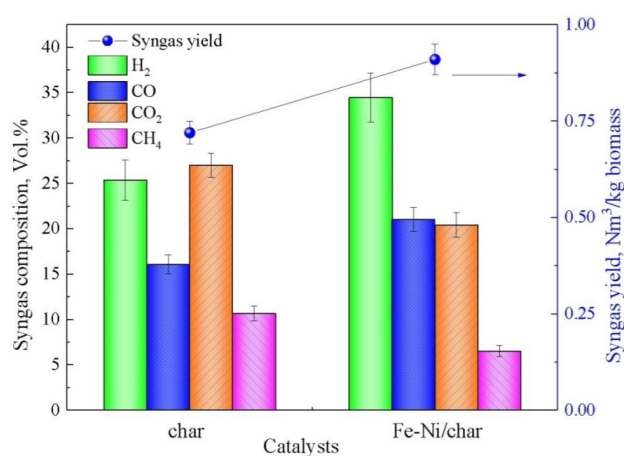


Figure 3. Syngas yield and composition with different catalysts.

3.3. Tar Yield, Conversion Efficiency, and Composition Analysis

The results of tar yield and conversion efficiency under different char-based catalysts by ex situ catalytic pyrolysis are described in Figure 4. In the absence of a catalyst, the tar yield is 287.5 g/kg biomass, while with char as a catalyst in the catalytic pyrolysis process, the tar yield is 147.25 g/kg biomass. The tar conversion efficiency is 48.78%, indicating that the char has fair catalytic activity as a catalyst, which is due to its inherent catalytic alkali and alkaline earth metallic, as well as the defected carbon structural units in chars [18]. Moreover, it can be seen intuitively that the Fe-Ni/char catalyst has significantly higher catalytic activity than the char catalyst, and the tar conversion efficiency is significantly increased (84.97 wt.%), which indicates that the Fe-Ni/char catalyst indeed has higher tar catalytic decomposition performances. The results indicated that the gas yields of char and Fe-Ni/char as catalysts at 800 °C were 0.72 and 0.91 Nm³/kg, tar yields were 147.25 and 43.21 g/kg, and char yields were 220 and 130 g/kg, respectively. In the previous studies, Shen et al. [43] used rice-husk-char-supported nickel-iron catalysts for catalytic cracking tar, and the results showed that the tar conversion efficiency was the best (93%) when the Ni-Char was used as catalyst. In their studies, the monometallic catalysts and bimetallic catalysts also presented high tar conversion efficiency (>80%), indicating that char could be used as a green solid resource in applications for energy recovery.

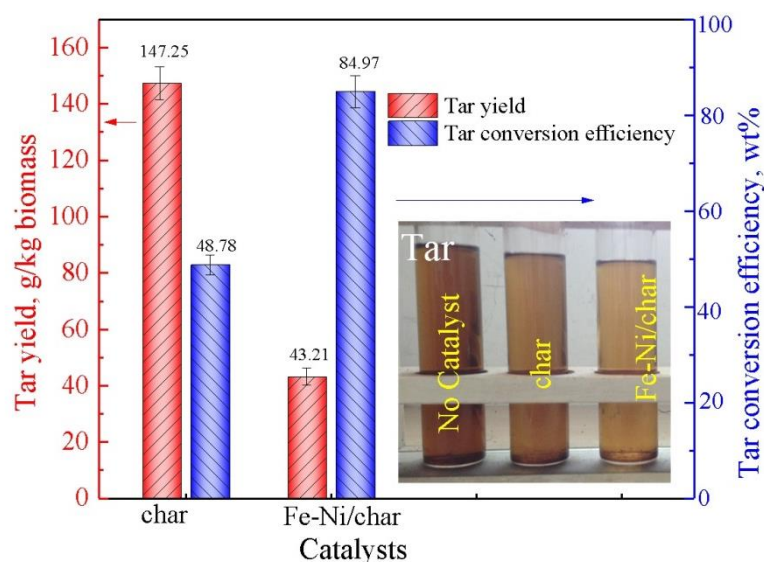


Figure 4. Tar yield and conversion efficiency.

In addition, under the ex situ conditions, the volatiles from the primary pyrolysis furnace enters the catalyst furnace and reaction with the catalyst, which further decomposes the oxygen-containing functional groups in the volatiles, and the acid sites in the catalyst surface can promote various secondary reactions releases of H₂O and CO₂, reduce the tar content, and increase the amount of small hydrocarbon compounds.

The ultimate analysis results of tar under different catalyst conditions are shown in Table 3. The two main elements in tar are C and O, followed by H and N, and only a small amount of S (0.023–0.048 wt%) has been detected. This result indicates that the concern about SO_x emissions or corrosion during tar use is negligible. Assuming that the S element is ignored, the molecular formula of tar can be written as CH_xO_yN_z, based on a C atom, and the results are also presented in Table 3. It can be seen that, after catalytic pyrolysis, the content of C increased dramatically, and the content of N and O decreased significantly, while the content of H and S changed slightly. The C content in the catalyst increased from 54.67 to 77.43 wt.%, the O content was reduced from 31.863 to 11.856 wt.%, and the O/C molar ratio was significantly reduced from 0.43 (without catalyst) to 0.115 (Fe-Ni/char). The decreased in O/C molar ratio indicated that the O-containing compounds in tar decreased after catalytic pyrolysis.

Meanwhile, compared with the case of no catalyst, the molar ratio of H/C in its produced tar decreased for all the tested catalysts. As shown in Figure 3, the yield of syngas increases after catalytic pyrolysis, which reduced the H/C molar ratio and derived the tar decomposition. Moreover, the N contents in these tars are high, especially in the condition of no catalyst (6.2 wt.%), indicating that there is a potential risk of polluting by the NO_x when utilizing these tars. After catalytic pyrolysis, the N content decreased in each catalyst, possibly due to the conversion of N-containing compounds to NO_x. Actually, mineral matters, such as potassium, calcium, iron, aluminum, etc., in biomass/char have great effects on N-conversion to NO_x [44]. Yi et al. [45] investigated the influence of mixed-Fe/Ca additives on nitrogen transformation during protein and amino acids pyrolysis, and the results indicated that the calcium can promote NH₃ formation and iron increases HCN yield. The synergistic effects of mixed-Fe/Ca additives enhanced the removal of HCN and NH₃. Meanwhile, Meesuk et al. [46] studied the catalytic reforming of nitrogen-containing volatiles evolved through pyrolysis of composed pig manure and revealed that Ni-based catalysts have high activity for conversion of nitrogen species in volatiles into N₂.

Table 3. Elemental analysis of tars from different catalysts.

Catalyst	C	H	N	S	O ^a	H/C ^b	O/C ^b	Molecular Formula
	wt. %							
No catalyst	54.67	7.219	6.2	0.048	31.863	1.585	0.437	CH _{1.585} O _{0.437} N _{0.097}
Char	57.45	7.04	5.43	0.023	30.057	1.47	0.392	CH _{1.471} O _{0.392} N _{0.097}
Fe-Ni/char	77.43	6.13	4.56	0.024	11.856	0.95	0.115	CH _{0.95} O _{0.114} N _{0.069}

^a By difference; ^b Molar ratio.

Supplementary Materials Table S1 shows the GC–MS analyses' results of main compounds identified in the tar. It should be noted that only the matched-degrees $\geq 90\%$ are listed in the results. About 100 compounds are tentatively identified, which can be divided into three groups: aromatic hydrocarbons, oxygenated compounds, and nitrogenous compounds.

It can be seen that catalytic pyrolysis with the char and Fe-Ni/char catalysts generated a higher percentage of aromatic hydrocarbons, compared with no catalyst pyrolysis, indicating that employed catalyst increases the percentage of aromatic hydrocarbons composition in the tar. Vichaphund et al. [47] also confirmed that the content of aromatic hydrocarbons in tar from *Jatropha* residues was increased under the condition of fast catalytic pyrolysis. The formation of aromatic hydrocarbons could be beneficial to improve calorific values of tar. In this study, aromatic hydrocarbons are composed of monocyclic aromatic hydrocarbons (MAHs) and polycyclic aromatic hydrocarbons (PAHs), where PAHs could be divided into light polyaromatic hydrocarbons (LPAHs) (two to three rings) and heavy polyaromatic hydrocarbons (HPAHs) (larger than three rings). As shown in Supplementary Materials Table S1, under the no-catalyst condition, the main components' MAHs in tar include benzene derivatives, while LPAHs include naphthalene derivatives, fluorene, and anthracene derivatives; and HPAHs include fluoranthene, pyrene-1-methyl, and triphenylene. The total content of HPAHs is 0.6828%. After catalytic pyrolysis, the total content of HPAHs is as the order of 0.5408% (char as catalyst) > 0.4089% (Fe-Ni/char as catalyst). It is obvious that HPAHs can condense at a high temperature with low concentration. After catalytic pyrolysis, the content of HPAHs in the tar is continuously reduced, which is beneficial to the subsequent treatment, making it more easy and efficient. In addition, it is also found that the molecular weight of tar decreased, which is consistent with the conclusions of ultimate analyses (Table 3). Obviously, the total contents of MAHs are higher than that of PAHs under all experimental conditions. The reason should be due to the formation of PAHs mainly derived from a series of reactions between MAHs and another oxygenate through the loss of H₂O and CO. Furthermore, PAHs are easily deposited on the surface of the catalyst to form coke.

In this study, the main oxygen-containing compounds in tar included aldehydes, ketones, phenols, ethers, and esters. The incontrovertible fact is that the presence of aldehydes and ketones

in the tar results in instability, while ethers and ester can reduce the calorific value of the tar. It can be seen from Supplementary Materials Table S1 that, when the catalyst is used, the percentage of oxygenated compounds shows a downward trend, indicating the occurrence of deoxygenation reactions (remove oxygen as CO, CO₂, and H₂O). For example, ketones might transform into aromatics and H₂O through condensation and decomposition reactions, while aldehydes might occur through dehydration reaction, and ester might occur through decarboxylation reactions with char-based catalysts. Especially, when Fe-Ni/char is used as a catalyst, the percentage of oxygenated compounds is only 7.9777%, which shows a significant decline compared with that in the no-catalyst pyrolysis (17.2932%). This is mainly due to the fact that the Ni can enhance the cracking of O–H, C–H, and C–C and have high selectivity for hydrodeoxygenation of various C–O and C=O bonds during the tar upgrading process [48]. Compared with no catalyst pyrolysis, catalytic pyrolysis mainly generated ethyl acetate, while no methyl propionate was generated. This could be due to the methyl propionate being converted to ethyl acetate by the isomerization reaction. Meanwhile, the percentages of phenolics in tars after catalytic pyrolysis were all decreased, indicating that the hydrocarbons might have been produced from phenolics.

The nitrogenous compounds in this study mainly consist of pyrimidine, pyrazine, pyridine, pyrrole, quinolone, and nitrile, which, due to the occurrence forms of nitrogen in biomass, mainly exist in the protein, accounting for 80–85% of total nitrogen in biomass [44]. Nitrogenous compounds in tar may cause potential NO_x pollution during combustion. As can be seen from Supplementary Materials Table S1, after catalytic pyrolysis, all the percentages of nitrogenous compounds are decreased significantly, especially under the Fe-Ni/char catalysts' conditions, indicating that the char-supported Fe-Ni catalyst can improve the quality of the tar. Meanwhile, compared with the char as catalyst, the percentage of nitrogenous compounds is 1.9657% when Fe-Ni/char is used as the catalyst, which less than 2.6707%. This result indicates the Fe-Ni-metals-loaded char catalyst facilitates thermal cracking of nitrogenous compounds with the release of gas-N [45].

In conclusion, the improvement of tar quality in this study was achieved through ex situ catalytic pyrolysis of biomass on a char-based catalyst. At the same time, with the decrease of the content of oxygen-containing compounds and nitrogen-containing compounds, the content of aromatic hydrocarbons is higher, indicating that the char-supported Ni and Fe catalysts are beneficial to improving the quality of pyrolytic tar.

3.4. XPS Analyses of Catalyst

In order to investigate the surface valence states of the characteristic elements in the catalysts before and after reactions, XPS measurement is employed. The high-resolution XPS scans of the C 1s, Fe 2p and Ni 2p regions for the representative catalyst Fe-Ni/char are depicted in Figure 5. The C 1s spectrum of fresh Fe-Ni/char catalyst is deconvoluted into the carbon atom in the form of sp² hybridized graphitized carbon (C–C) (Figure 5a). The peak at the binding energy of about 284.5 eV indicated that the most carbons in the char-supported catalyst are aromatic carbons. Garcia-Bordeje et al., [49] studied the hydrothermal carbonization of cellulose and found that a prominent signal of sp² carbons in aromatic rings, consistent with the observation in this work. After catalytic pyrolysis, a peak at the binding energy of 288.43 eV of C 1s appeared which correspond to carboxyl group (COOR). The reason of this changed might be attributed to the tar is decomposed to form coke and deposited on the surface of char.

The Fe 2p spectrum of before and after reaction Fe-Ni/char comprises two and three peaks with differentiated binding energy values, respectively (see Figure 5b). Usually, the peak position of Fe 2p_{1/2} and Fe 2p_{3/2} determines the ionic states of Fe. Meanwhile, the satellite peak positions for the Fe 2p_{1/2} and Fe 2p_{3/2} peaks are very sensitive to the oxidation states. Therefore, these peaks could be used for determining the ionic states of iron. Before catalytic pyrolysis, the Fe 2p_{3/2} with binding energy of 711.28 eV identified as the peak of FeO(OH) or other substances between Fe₂O₃ and FeO(OH), while the Fe 2p_{1/2} peak at a binding energy of 724.49 eV is ascribed to Fe³⁺ cations. After

catalytic pyrolysis, a peak of Fe 2p_{3/2} with binding energy of 710.65 eV indicated that both Fe²⁺ and Fe³⁺ should exist. The shifts from 711.28 to 710.65 eV indicate a reduction of Fe³⁺ to Fe²⁺ during the catalytic pyrolysis process. Noteworthy, after catalytic pyrolysis, a peak at binding energy of 719.33 eV appears which associated with Fe⁰. This result manifests that there were oxidation-reduction reactions during the catalytic pyrolysis process. The iron oxide could be reduced by carbon and/or reducing gas (H₂, CO), which comes from biomass pyrolysis.

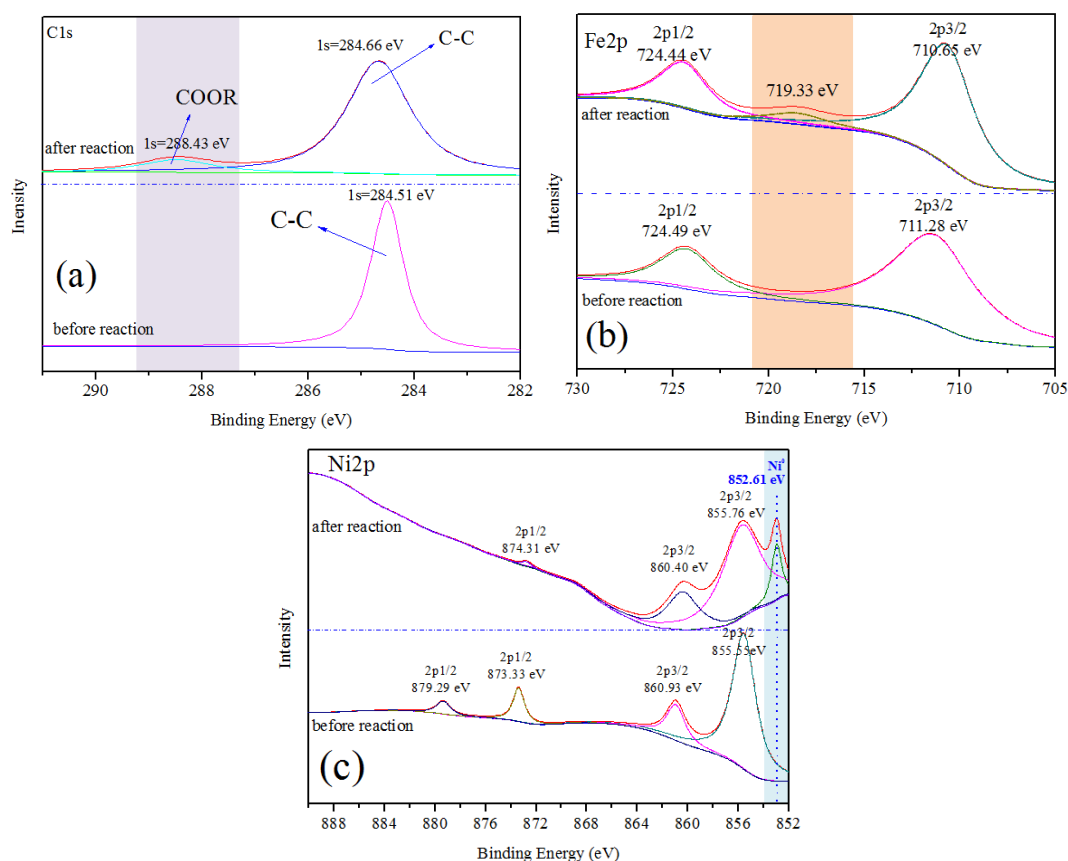


Figure 5. XPS patterns of Fe-Ni/char catalyst before and after reaction. (a) C1s spectra; (b) Fe2p spectra; (c) Ni2p spectra.

In the Ni 2p spectrum (Figure 5c), before catalytic pyrolysis, there are four peaks with the binding energy in the range of about 855–879 eV. The Ni 2p_{3/2} with binding energy of 855.55 eV identified as the peak of Ni(OH)₂, while the Ni 2p_{1/2} with the binding energy of 873.33 and 879.29 eV could be assigned to Ni²⁺ on the surface of catalyst. Usually, the binding energy of NiO usually distributes at 853.3 eV in the standard spectrum. However, the Ni 2p_{3/2} peak of before and after reaction catalysts centered at 855.55 and 855.76 eV, respectively, which can be attributed to the interaction with the catalyst support indicating the presence of NiO or other nickel compounds. After catalytic pyrolysis, a special peak is observed at binding energy of 852.61 eV, which can be attributed to metal Ni. Carbothermal and hydrogenation reductions of Ni²⁺ to Ni should be the main reasons.

3.5. Tar Catalytic Conversion Mechanisms

In order to more clearly understand the catalytic pyrolysis process of the tar, based on the above discussion, the main reactions pathway involved during ex situ catalytic pyrolysis of biomass is summarized in Figure 6. For ex situ catalytic pyrolysis process, biomass pyrolysis is the first step. Cellulose, hemicellulose, and lignin are the three main components in biomass. Cellulose, as the main component of lignocellulosic biomass, can form furan compounds through a series of dehydration,

cracking, decarboxylation, and decarboxylation reactions during thermal degradation. As such, it is evidenced that hemicellulose was likely to be depolymerized into furan compounds, which is comparable with the result of cellulose degradation. Unlike cellulose and hemicellulose, lignin is primarily decomposed into phenolic compounds. During the above pyrolysis process, non-condensable gas and a solid residue called char are also produced.

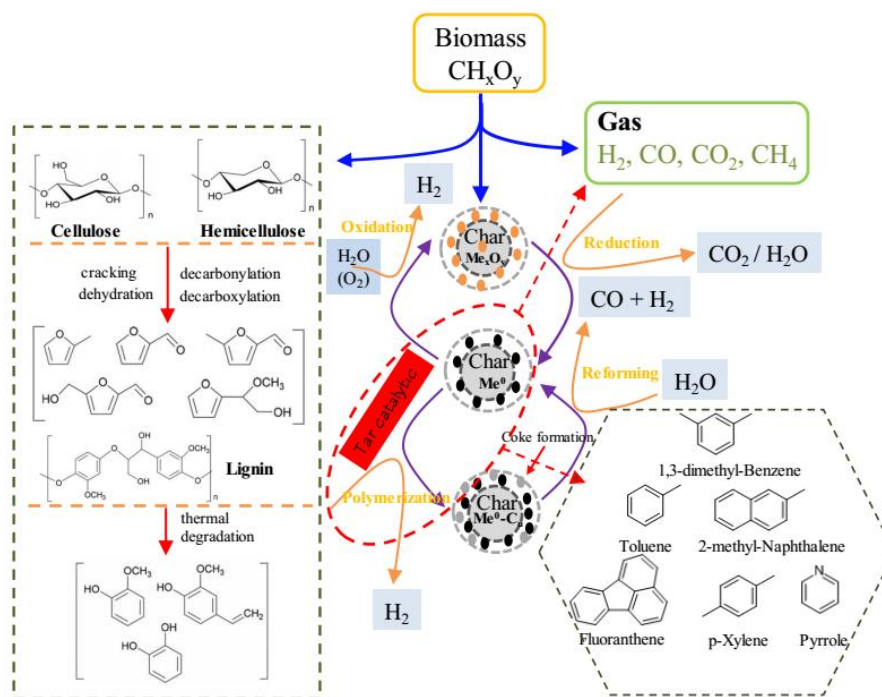


Figure 6. Proposed reaction pathway for ex situ catalytic pyrolysis of biomass.

The pyrolysis vapors then pass through the catalyst bed and undergo the catalyst pyrolysis upgrading. In this study, char-supported Fe/Ni catalysts were employed. According to the XPS analysis results, Fe and Ni are existed in the form of oxidation state in fresh catalysts (Me_xO_y refers to metallic oxides, and M refers to Fe, Ni). When the non-condensable gases which contain reducing gas (H_2 , CO) pass through the catalyst bed, the Me_xO_y is reduced to Me^0 . Meanwhile, the condensable gases (refer to tar) are adsorbed on the surface of char-supported catalysts. The reduced metal Me^0 active sites at the catalysts' surface catalyze the reaction of polymerization of tars which lead to coke formation and deposit on the catalysts, as well as generate H_2 . The formed coke could be reacted with steam to produce CO and H_2 by steam reforming. In addition, the Me^0 in the oxidizing atmosphere can be oxidized, giving rise to different valence states in metal oxides.

4. Conclusions

Ex situ catalytic pyrolysis of biomass for syngas production and tar decomposition based on char-supported Fe and Ni catalyst was investigated. Ni/char catalyst exhibited the highest catalytic performance: The syngas yield and the molar ratio of H_2/CO were $0.91 \text{ Nm}^3/\text{kg}$ biomass and 1.64, respectively. Moreover, the lowest tar yield (43.21 g/kg biomass) and the highest tar catalytic conversion efficiency (84.97 wt.%) were also obtained under the condition of Fe-Ni/char. After catalytic pyrolysis, the percentage of aromatic hydrocarbons in tar dramatically increased with the significant decrease in oxygenated compounds and nitrogenous compounds, especially in the presence of Fe-Ni/char catalyst. The XPS analysis results indicated that the metallic oxides (Me_xO_y) were reduced to metallic Me^0 after catalytic pyrolysis promoted the increase of tar conversion.

Supplementary Materials: The following are available online at <http://www.mdpi.com/2079-4991/10/7/1397/s1>. Figure S1: SEM-EDS of different fresh catalysts. (a) char, (b) Fe-Ni/char. Figure S2: Pore size distributions and nitrogen adsorption-desorption isotherms of different fresh catalysts. (a) char, (b) Fe-Ni/char. Table S1. Main compounds identified in the tar product by GC-MS analysis

Author Contributions: Conceptualization, M.H. and D.G.; software, S.L.; investigation, M.H.; data curation, M.H.; writing—original draft preparation, M.H. and D.G.; writing—review and editing, M.H. and B.C.; funding acquisition, B.X. All authors have read and agreed to the published version of the manuscript.

Funding: This research was funded by National Natural Science Foundation of China, China (21706087), China Postdoctoral Science Foundation, China (2019T120658, 2018M640703), and National Key Research and Development Project, China (2018YFB1502900).

Acknowledgments: The authors would also like to thank the analytical and test center of HUST for carrying out the analysis of the samples.

Conflicts of Interest: The authors declare no conflict of interest.

References

1. Hu, Q.; Shen, Y.; Chew, J.W.; Ge, T.; Wang, C. Chemical looping gasification of biomass with Fe₂O₃/CaO as the oxygen carrier for hydrogen-enriched syngas production. *Chem. Eng. J.* **2020**, *379*, 122346. [[CrossRef](#)]
2. Yin, Z.; Zhu, L.; Li, S.; Hu, T.; Chu, R.; Mo, F.; Hu, D.; Liu, C.; Li, B. A comprehensive review on cultivation and harvesting of microalgae for biodiesel production: Environmental pollution control and future directions. *Bioresour. Technol.* **2020**, *301*, 122804. [[CrossRef](#)]
3. Díaz-Pérez, M.A.; Serrano-Ruiz, J.C. Catalytic Production of Jet Fuels from Biomass. *Molecules* **2020**, *25*, 802. [[CrossRef](#)] [[PubMed](#)]
4. Zhang, Q.; Yu, Z.; Jin, S.; Zhu, L.; Liu, C.; Zheng, H.; Zhou, T.; Liu, Y.; Ruan, R. Lignocellulosic residue as bio-carrier for algal biofilm growth: Effects of carrier physicochemical properties and toxicity on algal biomass production and composition. *Bioresour. Technol.* **2019**, *293*, 122091. [[CrossRef](#)]
5. Zhang, Q.; Yu, Z.; Zhu, L.; Ye, T.; Zuo, J.; Li, X.; Xiao, B.; Jin, S. Vertical-algal-biofilm enhanced raceway pond for cost-effective wastewater treatment and value-added products production. *Water Res.* **2018**, *139*, 144–157. [[CrossRef](#)]
6. Ji, B.; Zhang, M.; Gu, J.; Ma, Y.; Liu, Y. A self-sustaining synergetic microalgal-bacterial granular sludge process towards energy-efficient and environmentally sustainable municipal wastewater treatment. *Water Res.* **2020**, *179*, 115884. [[CrossRef](#)]
7. Yang, Q.; Liang, J.; Li, J.; Yang, H.; Chen, H. Life cycle water use of a biomass-based pyrolysis polygeneration system in China. *Appl. Energy* **2018**, *224*, 469–480. [[CrossRef](#)]
8. Hu, M.; Laghari, M.; Cui, B.; Xiao, B.; Zhang, B.; Guo, D. Catalytic cracking of biomass tar over char supported nickel catalyst. *Energy* **2018**, *145*, 228–237. [[CrossRef](#)]
9. Hu, Q.; Dai, Y.; Wang, C. Steam co-gasification of horticultural waste and sewage sludge: Product distribution, synergistic analysis and optimization. *Bioresour. Technol.* **2020**, *301*, 122780. [[CrossRef](#)]
10. Guo, D.; Hu, M.; Chen, Z.; Cui, B.; Zhang, Q.; Liu, Y.; Luo, S.; Ruan, R.; Liu, Y. Catalytic Pyrolysis of rain tree biomass with nano nickel oxide synthesized from nickel plating slag: A green path for treating waste by waste. *Bioresour. Technol.* **2020**, 123831. [[CrossRef](#)]
11. Ding, Y.; Huang, B.; Li, K.; Du, W.; Lu, K.; Zhang, Y. Thermal interaction analysis of isolated hemicellulose and cellulose by kinetic parameters during biomass pyrolysis. *Energy* **2020**, *195*, 117010. [[CrossRef](#)]
12. Wang, Y.; Wu, Q.; Dai, L.; Zeng, Z.; Liu, Y.; Ruan, R.; Fu, G.; Yu, Z.; Jiang, L. Co-pyrolysis of wet torrefied bamboo sawdust and soapstock. *J. Anal. Appl. Pyrolysis* **2018**, *132*, 211–216. [[CrossRef](#)]
13. Chen, Z.; Lei, J.; Li, Y.; Su, X.; Hu, Z.; Guo, D. Studies on thermokinetic of *Chlorella pyrenoidosa* devolatilization via different models. *Bioresour. Technol.* **2017**, *244*, 320–327. [[CrossRef](#)] [[PubMed](#)]
14. Fahmy, T.Y.A.; Fahmy, Y.; Mobarak, F.; El-Sakhawy, M.; Abou-Zeid, R.E. Biomass pyrolysis: Past, present, and future. *Environ. Dev. Sustain.* **2020**, *22*, 17–32. [[CrossRef](#)]
15. Valderrama Rios, M.L.; González, A.M.; Lora, E.E.S.; Almazán Del Olmo, O.A. Reduction of tar generated during biomass gasification: A review. *Biomass Bioenergy* **2018**, *108*, 345–370. [[CrossRef](#)]
16. Zhang, X.; Deng, H.; Hou, X.; Qiu, R.; Chen, Z. Pyrolytic behavior and kinetic of wood sawdust at isothermal and non-isothermal conditions. *Renew. Energy* **2019**, *142*, 284–294. [[CrossRef](#)]

17. Kay Lup, A.N.; Abnisa, F.; Daud, W.M.A.W.; Aroua, M.K. A review on reaction mechanisms of metal-catalyzed deoxygenation process in bio-oil model compounds. *Appl. Catal. A Gen.* **2017**, *541*, 87–106. [[CrossRef](#)]
18. Chen, W.; Li, K.; Xia, M.; Yang, H.; Chen, Y.; Chen, X.; Che, Q.; Chen, H. Catalytic deoxygenation co-pyrolysis of bamboo wastes and microalgae with biochar catalyst. *Energy* **2018**, *157*, 472–482. [[CrossRef](#)]
19. Shafaghat, H.; Rezaei, P.S.; Ro, D.; Jae, J.; Kim, B.; Jung, S.; Sung, B.H.; Park, Y.-K. In-situ catalytic pyrolysis of lignin in a bench-scale fixed bed pyrolyzer. *J. Ind. Eng. Chem.* **2017**, *54*, 447–453. [[CrossRef](#)]
20. Hu, M.; Chen, Z.; Wang, S.; Guo, D.; Ma, C.; Zhou, Y.; Chen, J.; Laghari, M.; Fazal, S.; Xiao, B.; et al. Thermogravimetric kinetics of lignocellulosic biomass slow pyrolysis using distributed activation energy model, Fraser–Suzuki deconvolution, and iso-conversional method. *Energy Convers. Manag.* **2016**, *118*, 1–11. [[CrossRef](#)]
21. Chen, Z.; Hu, M.; Zhu, X.; Guo, D.; Liu, S.; Hu, Z.; Xiao, B.; Wang, J.; Laghari, M. Characteristics and kinetic study on pyrolysis of five lignocellulosic biomass via thermogravimetric analysis. *Bioresour. Technol.* **2015**, *192*, 441–450. [[CrossRef](#)] [[PubMed](#)]
22. Choi, G.; Oh, S.; Kim, J. Clean pyrolysis oil from a continuous two-stage pyrolysis of scrap tires using in-situ and ex-situ desulfurization. *Energy* **2017**, *141*, 2234–2241. [[CrossRef](#)]
23. Fan, L.; Ruan, R.; Li, J.; Ma, L.; Wang, C.; Zhou, W. Aromatics production from fast co-pyrolysis of lignin and waste cooking oil catalyzed by HZSM-5 zeolite. *Appl. Energy* **2020**, *263*, 114629. [[CrossRef](#)]
24. Fan, L.; Chen, P.; Zhou, N.; Liu, S.; Zhang, Y.; Liu, Y.; Wang, Y.; Omar, M.M.; Peng, P.; Addy, M.; et al. In-situ and ex-situ catalytic upgrading of vapors from microwave-assisted pyrolysis of lignin. *Bioresour. Technol.* **2018**, *247*, 851–858. [[CrossRef](#)] [[PubMed](#)]
25. Han, J.; Wang, X.; Yue, J.; Gao, S.; Xu, G. Catalytic upgrading of coal pyrolysis tar over char-based catalysts. *Fuel Process. Technol.* **2014**, *122*, 98–106. [[CrossRef](#)]
26. Gamliel, D.P.; Du, S.; Bollas, G.M.; Valla, J.A. Investigation of in situ and ex situ catalytic pyrolysis of miscanthus × giganteus using a PyGC–MS microsystem and comparison with a bench-scale spouted-bed reactor. *Bioresour. Technol.* **2015**, *191*, 187–196. [[CrossRef](#)] [[PubMed](#)]
27. Koido, K.; Watanabe, Y.; Ishiyama, T.; Nunoura, T.; Dowaki, K. Fate of sulphur during simultaneous gasification of lignin-slurry and removal of hydrogen sulphide over calcium aluminate supported nickel oxide catalyst. *J. Clean. Prod.* **2017**, *141*, 568–579. [[CrossRef](#)]
28. Ouedraogo, A.S.; Bhoi, P.R. Recent progress of metals supported catalysts for hydrodeoxygenation of biomass derived pyrolysis oil. *J. Clean. Prod.* **2020**, *253*, 119957. [[CrossRef](#)]
29. Furusawa, T.; Tsutsumi, A. Comparison of Co/MgO and Ni/MgO catalysts for the steam reforming of naphthalene as a model compound of tar derived from biomass gasification. *Appl. Catal. A Gen.* **2005**, *278*, 207–212. [[CrossRef](#)]
30. Moud, P.H.; Andersson, K.J.; Lanza, R.; Engvall, K. Equilibrium potassium coverage and its effect on a Ni tar reforming catalyst in alkali- and sulfur-laden biomass gasification gases. *Appl. Catal. B Environ.* **2016**, *190*, 137–146. [[CrossRef](#)]
31. Cheah, S.; Gaston, K.; Parent, Y.O.; Jarvis, M.; Vinzant, T.B.; Smith, K.; Thornburg, N.E.; Nimlos, M.R.; Magrini-Bair, K.A. Nickel cerium olivine catalyst for catalytic gasification of biomass. *Appl. Catal. B Environ.* **2013**, *134–135*, 34–45. [[CrossRef](#)]
32. Mohammed, I.Y.; Abakr, Y.A.; Yusup, S.; Alaba, P.A.; Morris, K.I.; Sani, Y.M.; Kazi, F.K. Upgrading of Napier grass pyrolytic oil using microporous and hierarchical mesoporous zeolites: Products distribution, composition and reaction pathways. *J. Clean. Prod.* **2017**, *162*, 817–829. [[CrossRef](#)]
33. Hu, M.; Wang, X.; Chen, J.; Yang, P.; Liu, C.; Xiao, B.; Guo, D. Kinetic study and syngas production from pyrolysis of forestry waste. *Energy Convers. Manag.* **2017**, *135*, 453–462. [[CrossRef](#)]
34. Cheng, S.; Wei, L.; Julson, J.; Muthukumarappan, K.; Kharel, P.R. Upgrading pyrolysis bio-oil to hydrocarbon enriched biofuel over bifunctional Fe-Ni/HZSM-5 catalyst in supercritical methanol. *Fuel Process. Technol.* **2017**, *167*, 117–126. [[CrossRef](#)]
35. Wang, L.; Hisada, Y.; Koike, M.; Li, D.; Watanabe, H.; Nakagawa, Y.; Tomishige, K. Catalyst property of Co-Fe alloy particles in the steam reforming of biomass tar and toluene. *Appl. Catal. B Environ.* **2012**, *121–122*, 95–104. [[CrossRef](#)]
36. Sirous-Rezaei, P.; Oh, D.; Hong, Y.; Kim, Y.-M.; Jae, J.; Jung, S.-C.; Jeon, J.-K.; Park, Y.-K. In-situ catalytic co-pyrolysis of yellow poplar and high-density polyethylene over mesoporous catalysts. *Energy Convers. Manag.* **2017**, *151*, 116–122. [[CrossRef](#)]

37. Feng, D.; Zhao, Y.; Zhang, Y.; Zhang, Z.; Sun, S. Roles and fates of K and Ca species on biochar structure during in-situ tar H₂O reforming over nascent biochar. *Int. J. Hydrogen Energy* **2017**, *42*, 21686–21696. [[CrossRef](#)]
38. Luo, S.; Zeng, L.; Xu, D.; Kathe, M.; Chung, E.; Deshpande, N.; Qin, L.; Majumder, A.; Hsieh, T.-L.; Tong, A.; et al. Shale gas-to-syngas chemical looping process for stable shale gas conversion to high purity syngas with a H₂:CO ratio of 2:1. *Energy Environ. Sci.* **2014**, *7*, 4104–4117. [[CrossRef](#)]
39. De Sales, C.A.V.B.; Maya, D.M.Y.; Lora, E.E.S.; Jaén, R.L.; Reyes, A.M.M.; González, A.M.; Andrade, R.V.; Martínez, J.D. Experimental study on biomass (*eucalyptus* spp.) gasification in a two-stage downdraft reactor by using mixtures of air, saturated steam and oxygen as gasifying agents. *Energy Convers. Manag.* **2017**, *145*, 314–323. [[CrossRef](#)]
40. Biagini, E.; Barontini, F.; Tognotti, L. Gasification of agricultural residues in a demonstrative plant: Vine pruning and rice husks. *Bioresour. Technol.* **2015**, *194*, 36–42. [[CrossRef](#)]
41. Weiland, F.; Hedman, H.; Marklund, M.; Wiinikka, H.; Öhrman, O.; Gebart, R. Pressurized Oxygen Blown Entrained-Flow Gasification of Wood Powder. *Energy Fuels* **2013**, *27*, 932–941. [[CrossRef](#)]
42. He, M.; Xiao, B.; Liu, S.; Hu, Z.; Guo, X.; Luo, S.; Yang, F. Syngas production from pyrolysis of municipal solid waste (MSW) with dolomite as downstream catalysts. *J. Anal. Appl. Pyrolysis* **2010**, *87*, 181–187. [[CrossRef](#)]
43. Shen, Y.; Zhao, P.; Shao, Q.; Ma, D.; Takahashi, F.; Yoshikawa, K. In-situ catalytic conversion of tar using rice husk char-supported nickel-iron catalysts for biomass pyrolysis/gasification. *Appl. Catal. B Environ.* **2014**, *152–153*, 140–151. [[CrossRef](#)]
44. Ren, Q.; Zhao, C. Evolution of fuel-N in gas phase during biomass pyrolysis. *Renew. Sustain. Energy Rev.* **2015**, *50*, 408–418. [[CrossRef](#)]
45. Yi, L.; Liu, H.; Lu, G.; Zhang, Q.; Wang, J.; Hu, H.; Yao, H. Effect of Mixed Fe/Ca Additives on Nitrogen Transformation during Protein and Amino Acid Pyrolysis. *Energy Fuels* **2017**, *31*, 9484–9490. [[CrossRef](#)]
46. Meesuk, S.; Sato, K.; Cao, J.; Hoshino, A.; Utsumi, K.; Takarada, T. Catalytic reforming of nitrogen-containing volatiles evolved through pyrolysis of composted pig manure. *Bioresour. Technol.* **2013**, *150*, 181–186. [[CrossRef](#)]
47. Vichaphund, S.; Aht-ong, D.; Sricharoenchaikul, V.; Atong, D. Production of aromatic compounds from catalytic fast pyrolysis of Jatropha residues using metal/HZSM-5 prepared by ion-exchange and impregnation methods. *Renew. Energy* **2015**, *79*, 28–37. [[CrossRef](#)]
48. Kay Lup, A.N.; Abnisa, F.; Wan Daud, W.M.A.; Aroua, M.K. A review on reactivity and stability of heterogeneous metal catalysts for deoxygenation of bio-oil model compounds. *J. Ind. Eng. Chem.* **2017**, *56*, 1–34. [[CrossRef](#)]
49. García-Bordejé, E.; Pires, E.; Fraile, J.M. Parametric study of the hydrothermal carbonization of cellulose and effect of acidic conditions. *Carbon* **2017**, *123*, 421–432. [[CrossRef](#)]

